IEEE Access
Multidisciplinary | Rapid Review | Open Access Journal

Received March 20, 2021, accepted April 22, 2021, date of publication April 30, 2021, date of current version June 2, 2021.

Digital Object Identifier 10.1109/ACCESS.2021.3076799

Laser Speckle Contrast Imaging Based on a Mobile Phone Camera

PING KONG[1], HAO XU[2], RAN LI[2], GANG HUANG[1], AND WEI LIU[3]

[1]Shanghai Key Laboratory of Molecular Imaging, Shanghai University of Medicine and Health Sciences, Shanghai 201318, China
[2]School of Medical Instrument and Food Engineering, University of Shanghai for Science and Technology, Shanghai 200093, China
[3]School of Internet of Things Engineering, Binjiang College of Nanjing University of Information Science and Technology, Wuxi 214105, China

Corresponding authors: Gang Huang (huanggang@sumhs.edu.cn) and Wei Liu (liuyiwei1030@hotmail.com)

This work was supported in part by the National Natural Science Foundation of China under Grant 11902190, in part by the Climbing Program from SUMHS under Grant B3-0200-20-311007, in part by the Construction Project of Shanghai Key Laboratory of Molecular Imaging under Grant 18DZ2260400, in part by the Shanghai Municipal Education Commission (Class II plateau disciplinary construction program of medical technology of SUMHS, 2018–2020), and in part by the Key Program of the National Natural Science Foundation of China under Grant 81830052.

ABSTRACT Laser speckle contrast imaging (LSCI) technology, a type of blood flow monitoring technology, has broad application prospects and has become an attractive subject of research. In recent years, with the popularization of smart phones, mobile healthcare has gradually entered the lives of the general public. In this paper, a camera system used on smart phones was employed to replace the industrial camera on the traditional laser speckle perfusion imager, and the quality of blood flow imaging was improved. Since the difference between the static and dynamic region of the raw speckle image can be reflected in the subbands of wavelet decomposition, the image processing can be performed while retaining the velocity information. Further, a speckle contrast analysis method based on mobile phone cameras is proposed; the method first processes the raw speckle images with a two-dimensional discrete wavelet transform and image interpolation and then performs a morphological operation. This method improved the speckle image contrast resolution and improved the visualization of images. The results showed that the contrast-to-noise ratio (CNR) of the blood perfusion image processed by the new method can be increased by up to 128%.

INDEX TERMS Laser speckle contrast imaging, image enhancement, mobile phone camera.

I. INTRODUCTION

Human microcirculation information reflects the physiological and pathological changes in the overall human body and local regions thereof and plays an extremely important role in understanding organ functions and discovering and diagnosing various diseases [1]. Among noninvasive microcirculation assessment technologies, laser speckle contrast imaging (LSCI) is a full-field, real-time and high-spatial-temporal-resolution optical imaging method [2]. This method can obtain a two-dimensional spatial map of the relative blood flow velocity in a wide field of view without scanning to detect the dynamic changes in blood flows [3], [4].

The traditional LSCI system is too expensive and cumbersome to be widely available and cannot be used flexibly in various scenarios [5]. Therefore, in the past several years, some researchers have begun to study using portable devices to conduct LSCI [6]. Richards *et al.* used an 8-bit webcam ($35) and a 14-bit industrial camera ($2000) for *in vivo* and *in vitro* experiments, respectively, and suggested that the LSCI results obtained by using a low-cost device are similar to those obtained by using traditional instruments; however, the bit depth of the image and sensitivity to small changes in blood flows are limited [7]. Jakovels *et al.* used a mobile phone camera instead of an industrial camera to conduct LSCI. Compared with a webcam, the LSCI method designed by Jakovels was determined to further improve portability. The experimental results showed that LSCI based on mobile phone cameras can be used for preliminary rapid monitoring related to skin blood flows [8]. However, in actual detection, the mobile phone camera also produces some ''false light intensity values'' due to the colour restoration algorithm of its image sensor [9], thereby causing large errors in the calculated blood flow images. To solve this problem, some scholars have successfully avoided the error caused by the camera algorithm by extracting the red component

The associate editor coordinating the review of this manuscript and approving it for publication was Vishal Srivastava.

of the bottom layer of the sensor and then calculating the speckle contrast [10]. However, this processing method also loses part of the speckle signal; this loss, in turn, leads to a reduction in the contrast resolution and visualization [11]. To collect more reliable physiological signals through mobile phone cameras, Tabei *et al.* processed the heart rate signals collected by sensors through a software-based method based on signal processing techniques/algorithms and finally calculated more accurate heart rates [12]. For speckle signals, some researchers used digital image processing technology to enhance speckle images, and then the blood flow images with higher contrast resolution and lower noise were calculated [13], [14].

In this study, the raw data of a mobile phone image sensor without additional filters were analysed and processed; thus, distortion of the speckle signal caused by the mobile phone image correction algorithm was avoided. In addition, a two-dimensional discrete wavelet transform (DWT) was used to decompose and enhance the image based on the high-frequency component of the speckle image in the blood flow area [15], thus improving the LSCI contrast resolution and blood flow visualization effect based on mobile phone cameras. Through these steps, the proposed new method can not only improve the portability of traditional devices, but also have a high-quality imaging on a mobile device. To test the effect, the blood flow simulation experiment and microcirculation perfusion experiment of an industrial camera and a mobile phone camera were conducted, and the processing effect of different methods was evaluated by comparing the contrast-to-noise ratio (CNR) and the distribution density of the contrast [16].

II. METHODS

A. PRINCIPLES AND METHODS

1) PRINCIPLE OF LSCI

Speckle is produced when coherent light is scattered from a random medium, and the scattered light produces a random interference pattern. The movement of the scattered particles in the random medium causes the phase of the scattered light to change, thereby changing the random interference pattern and producing time-varying speckles. In blood flow monitoring, red blood cells are the main scattering material, and the flow of red blood cells causes fluctuation in speckles [17], [18]. The fluctuation rate of speckle is proportional to the speed of scattering particles and can be captured by a CCD or CMOS camera into widefield images. Therefore, when the exposure time is determined, in areas with higher flow, speckles fluctuate faster, and the speckle image is blurred. The ''speckle contrast'' is usually used to quantitatively describe and analyse this blurring in the speckle images [19]; the speckle contrast is defined as the ratio of the standard deviation (SD) to the average intensity and calculated by

$$K = \frac{\sigma_s}{<I>} \tag{1}$$

where σ_s is the SD of the spatial intensity of the speckle and $<I>$ is the mean value of the spatial intensity of the speckle. A smaller K means that the speckle pattern is more blurred and the speed of the moving particles is faster. K is obtained by calculating the contrast value of the spatial sliding window (usually 5*5 px or 7*7 px), and the sliding window traverses the entire image to obtain a two-dimensional blood flow distribution image [20].

Since K is inversely proportional to the blood flow velocity, to facilitate data comparison, we assume that $1/K^2$ is the Blood Perfusion Index (BPI), which is positively correlated with the blood flow velocity. In this paper, the BPI was used in the comparison of LSCI speed, and K was used for statistics and analysis of the different methods.

2) SPECKLE CONTRAST ANALYSIS METHOD BASED ON A MOBILE PHONE CAMERA

The resolution of speckle images captured by mobile phone cameras is lower than that captured by industrial cameras; the blurring effect of speckle images is weakened, thus ultimately resulting in the loss of speckle signals. Therefore, digital image processing technology is needed to improve image resolution.

C. E. Perez-Corona *et al.* proposed a space-directional approach to calculate contrast images. Experimental results show that this method can achieve high noise attenuation and can produce a higher distance in value between the static and dynamic regions, thereby improving the visual discrimination between them [21]. However, the contrast calculation is not direct but involves directional analysis, so the processing time will increase and the number of valid computed pixels in the flow area is reduced.

P. Miao *et al.* proposed a registered laser speckle contrast analysis method to improve the distinguishability of small vessels and suppress the noise induced by respiration or heart beating [22]. In this method, a cubic basis-spline (B-spline) interpolator is used to register the raw speckle images. However, the interpolator takes the form of a low-pass filter that suppresses high-frequency components in varying degrees [23]. Therefore, in the raw speckle image, the high-frequency component corresponding to the static area is suppressed, and the range of contrast values is compressed.

F. Lopez-Tiro *et al.* proposed a methodology based on the DWT to improve the visualization of in vitro blood vessels. The focus of this method is to denoise the high frequency in contrast images and to visualize the contrast values after denoising in the class corresponding to the dynamic region [14]. However, the edges of blood vessels are also high-frequency components. When high-frequency information is eliminated, the edges of blood vessels tend to be irregular and jagged.

The static and dynamic regions of the raw speckle image correspond to the high-frequency and low-frequency components, respectively, and the difference can be reflected in the subbands of wavelet decomposition. Therefore, we used

a method combining a DWT and interpolation to improve the blood flow imaging quality of mobile phone cameras. On the one hand, image interpolation can be performed to compensate for insufficient resolution; on the other hand, there will be no loss of high-frequency information caused by smoothing effects in the image interpolation [24].

Various types of wavelets have become prevalent throughout the development of the DWT. One of the most important wavelets is the Haar wavelet, which can obtain a higher peak signal-to-noise ratio (PSNR) and lower mean square error (MSE) in image reconstruction [25], [26]. Moreover, since the Haar wavelet is both orthogonal and symmetric, it can obtain satisfactory results even in the presence of noise [27]. The Haar wavelet transform consists of a filter bank, a series of low-pass and high-pass filters [28]. The low- and high-pass filters are

$$L = \frac{1}{\sqrt{2}}(1 \quad 1) \tag{2}$$

$$H = \frac{1}{\sqrt{2}}(1 \quad -1) \tag{3}$$

Since the higher the level of decomposition, the less the low-frequency information contained, level-1 decomposition and the Haar wavelet were selected to decompose the image to obtain the approximate coefficient matrix LL and detail coefficient matrixes LH, HL, and HH [29]. The approximate coefficient matrix represents the low-frequency signal of the speckle image, and the detail coefficient matrix represents the high-frequency signal of the speckle image. Then, the bilinear interpolation and the nearest-neighbour interpolation were used for the low-frequency and high-frequency components, respectively, to avoid the information fusion between the dynamic and static speckle. This method does not need to strictly distinguish between and locate the areas of dynamic speckle and static speckle and can obtain more accurate speckle images with higher resolution.

In addition, the obtained contrast image was morphologically eroded. The morphological operation is a common image processing method [30] that can improve the clarity of the image structure. Erosion was used to eliminate background noise and refine the edge area of the image. In morphological operations, it is necessary to select structural elements and their sizes according to the actual image structure. In this paper, a circular structure with a radius of 2 pixels was used for the erosion calculation.

The complete processing steps are shown in Fig. 1. First, extract and integrate the red pixel components of the unprocessed raw data to obtain the rRAW data, and then decompose, interpolate and reconstruct the rRAW data by using a two-dimensional DWT to obtain the upsampled speckle image. The spatial contrast was calculated by (1), and finally, the obtained contrast image was transformed via morphological erosion. To facilitate the subsequent comparison and analysis, this complete step above was set as ep-LSCI (enhance phone-LSCI). Only three steps, namely, (a), (b), and (d), were performed, thus indicating that the steps without image

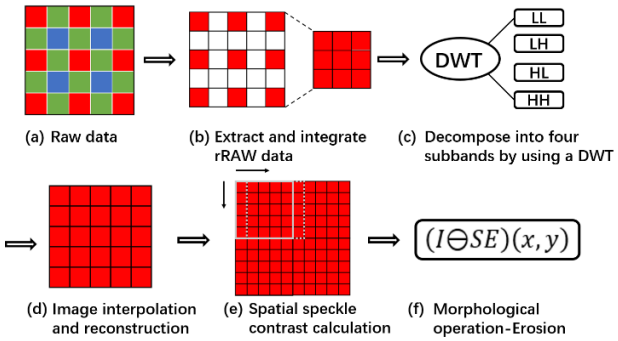

FIGURE 1. Flow chart of speckle contrast analysis based on a mobile phone camera. The whole process covers raw data conversion; red component extraction and integration; image decomposition, interpolation and reorganization; and finally, morphological changes. The contrast is calculated by the spatial contrast algorithm.

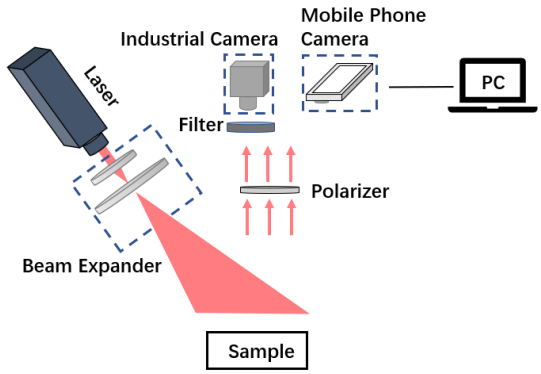

FIGURE 2. Schematic diagram of the LSCI experimental device.

enhancement were set as p-LSCI (phone-LSCI). The industrial camera experimental group was set as i-LSCI (industrial camera-LSCI).

3) CONTRAST-TO-NOISE RATIO

The CNR [31] can provide image quality information for some noisy images. The CNR can be used to calculate the change in the contrast between two regions of interest (ROIs) in an image. The CNR is defined as

$$CNR = \frac{\mu_{flood} - \mu_{background}}{\sigma_{background}} \tag{4}$$

where μ_{flood} and $\mu_{fbackground}$ are the mean values of the contrast of the blood flow area and the background area, respectively; and where $\sigma_{background}$ represents the SD of the contrast of the background area. The numerator of the equation represents the intensity of the signal (i.e., the difference between the contrast value of the blood flow and the background); and the denominator represents the noise intensity of the contrast. A higher CNR represents a greater contrast between the dynamic area and the static area and a better visualization quality. In the experiment, the background ROIs that are the same size as the ROIs in the flow area were used to calculate the background media.

B. EXPERIMENTAL DEVICES

The laser light source used in the experiment should be selected to irradiate the tissue to show high-scattering and low-absorption characteristics. The commonly used lasers are generally 632-nm red helium-neon lasers and 780-nm near-infrared lasers [32]. Some mobile phones have an IR-cut filter. To eliminate the influence of the filter, a 650 nm He-Ne laser was used in this experiment. The camera exposure time was set as 20 ms, and a narrow band filter (filtering 632 nm-668 nm) was installed in front of the industrial camera lens to filter out the interference of background light. The experimental device is shown in Fig. 2. Two types of devices were used to collect images separately, and the size of the collected speckles was two pixels by adjusting the focal length of the camera to ensure a fair comparison between the two devices. The names of the devices and their resolutions and pixel areas are listed in Table 1.

TABLE 1. Device parameters.

Device	Resolution	Pixel size (μm)	Sensor type
Mono-industrial camera (TXG14NIR, Baumer, Frauenfeld，Germany [34], [35])	1392*1040	6.45 *6.45	CCD
Phone camera (Sony IMX498 [36])	4608*3456	1.12*1.12	CMOS

The sensor of the mono-industrial camera is a fully transparent CCD sensor without a filter. This sensor has higher light input and sensitivity and has no algorithm influence. The light intensity information is well preserved; therefore, mono-industrial cameras are used as image acquisition devices in traditional laser speckle perfusion imagers. For mobile phone cameras, the reflected light through the optical lens first reaches the target surface of the CMOS sensor covered with the colour filter array (CFA) and generates electrical signals according to the light intensity. Next, the digital signal is transmitted to the image processing unit through amplifier amplification and analogue-to-digital conversion to generate raw image data. Finally, colour interpolation and postprocessing are required to obtain an image meeting people's visual perception [36]. In the mobile phone camera experimental group, the data analysed and processed is actually the red pixel data (rRAW) in the raw image. To obtain the rRAW data, the raw linear image data in the mobile phone camera sensor needs to be formatted with the open-source raw converter DCRam, and the red pixel components need to be extracted thereafter.

C. BLOOD FLOW SIMULATION EXPERIMENT

To test the imaging quality of LSCI achieved by using mobile phone cameras and industrial cameras, a set of blood flow simulation experiment devices was designed. In the experiments, industrial cameras and mobile phone cameras were used for image acquisition. The test sample was 2% homogenized milk, and the particle size was approximately 5-10 μm. The syringe was moved forward by a stepping motor in a transparent rubber tube. To perform different flow rate verification experiments, the flow rate of the solution was controlled by changing the speed of the stepper motor.

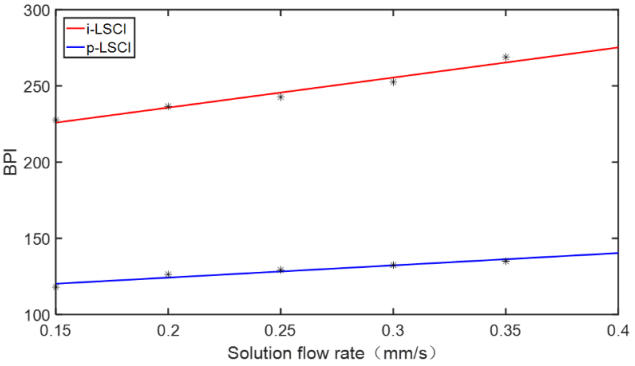

FIGURE 3. Comparison of LSCI speed measurement results obtained by using mobile phones and industrial cameras.

D. MICROCIRCULATION BLOOD PERFUSION EXPERIMENT

In the finger microcirculation blood perfusion [37] detection experiment, the laser was irradiated on the back of the subject's hand by using a beam expander. Next, the mobile phone camera and industrial camera were used to collect the reflected light, and the collected pictures and data were transferred to a computer for processing and analysis. The study protocols were approved by the hospital ethics committee. All participants signed an informed consent form.

III. EXPERIMENTAL RESULTS AND DISCUSSION

A. BLOOD FLOW SIMULATION SYSTEM

In Fig. 3, the x-axis shows the actual velocity of the solution flow, and the y-axis shows the Blood Perfusion Index (BPI) of the LSCI. The figure shows that as the solution flow rate increases, the BPI obtained by the two devices increases. Although industrial camera groups are more sensitive than mobile phone camera groups to changes in flow rates due to the different hardware sensors, the rising trend of the BPI can prove the feasibility of using mobile phone cameras for LSCI.

In the next step, the imaging effects of the two devices were studied and compared, and the ep-LSCI method was employed to enhance the images of the mobile phone camera group. Fig. 4 is a pseudocolour map of haemodynamics drawn from the contrast map, in which the speed range is set to 0-70 levels, red represents the area where the flow velocity is faster, and blue represents the area where the flow velocity is slow or static. In the results of the industrial camera group (shown in Fig. 4A), although there is a little noise near the flow area, the overall quality of the image is high, and the flow of the solution in the hose can be clearly shown. The results of the mobile phone camera group (shown in Fig. 4B) show that the background contains considerable noise, and the contrast between the flowing solution and the static background is not obvious. Fig. 4C is the blood flow image obtained by ep-LSCI processing. After image enhancement, the background noise

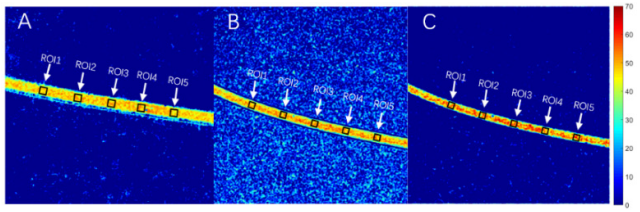

FIGURE 4. Blood flow images obtained by different LSCI methods. Panel A is the blood flow image obtained by i-LSCI processing, Panel B is the blood flow image obtained by p-LSCI processing, and Panel C is the blood flow image obtained by ep-LSCI processing.

TABLE 2. Comparison of the CNRs obtained by different LSCI methods.

LSCI Method	ROI1	ROI2	ROI3	ROI4	ROI5	Mean	SD
i-LSCI	5.53	5.54	5.45	5.51	5.4	5.48	0.002
p-LSCI	1.97	1.86	2.05	1.95	1.95	1.96	0.004
ep-LSCI	4.41	4.41	4.62	4.42	4.48	4.47	0.006

is significantly reduced. The specific enhancement effect is quantified and compared through CNR.

Table 2 shows the CNR values of the five ROIs marked in Fig. 4A. The results show that the CNR of the industrial camera group is the highest and that of the mobile phone camera group is the lowest. After image enhancement, the CNR of ep-LSCI is improved by 128% compared to that of p-LSCI; the CNR of ep-LSCI is close to the result of the industrial camera group. This finding shows that the method is effective in enhancing the mobile phone camera group; this enhancement is conducive to positioning blood vessels more precisely and identifying the blood flow velocity.

In addition, the experiment showed that the blood perfusion images obtained by different methods have different speed distributions in the hose. Part of the reason is that the LSCI method describes the blood flow velocity by calculating the speed of the scattering particles. Therefore, if the scattering particles in the solution are relatively dispersed or unevenly distributed, the obtained contrast value distribution will also be relatively dispersed. Another reason is related to the size of the pixel area of the image sensor. The smaller the pixel area is, the less light entering the sensor, and the worse the photosensitive performance. Table 1 shows that the light-sensitive area of the image sensor of the mobile phone camera is relatively small, and some speckle signals will be lost when the amount of light is insufficient during shooting, thus resulting in an unconcentrated contrast value distribution eventually.

To specifically test the distribution of the contrast values obtained by these three methods, a section of the hose (24*24 px) was selected to calculate the probability density of the contrast values in this area, and a normal distribution curve was obtained. In the normal distribution curve, μ represents the mean value of this set of data, determines the position of the peak of the curve, and is the central tendency of the normal distribution, which represents the final contrast result of a region. σ represents the SD of this set of data.

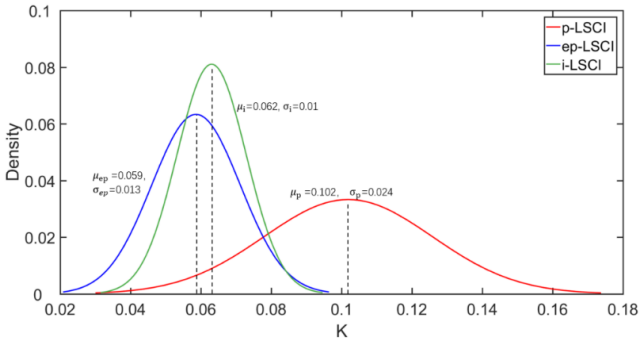

FIGURE 5. The normal distribution curve of the solution flow area.

The smaller the SD is, the shorter the distance between most variable values, thus indicating that most values are closely clustered around the mean. Conversely, the larger the SD is, the greater the degree of dispersion of the data, and the more likely errors are to occur during detection. As shown in Fig. 5, the mean values of the i-LSCI and p-LSCI curves are 0.062 and 0.102, respectively; and the SD are 0.01 and 0.024, respectively. For the ep-LSCI curve, the mean value is 0.059, which is significantly lower. This shows that through the ep-LSCI method, the speckle signal is enhanced and a higher BPI can be obtained; these results are helpful for us to identify and measure the velocity of the flow area. The SD of the enhanced ep-LSCI is 0.013, which is significantly lower than that of p-LSCI and is close to the result obtained by using an industrial camera. Therefore, with the ep-LSCI method, the intensity distribution of the obtained contrast is uniform, and the error is smaller; therefore, this method can be used to perform better blood flow imaging.

B. ANALYSIS OF THE MICROCIRCULATION BLOOD PERFUSION EXPERIMENT

First, an industrial camera is used to perform the LSCI detection on the microcirculation of the finger, and the result is shown in Fig. 6. The figure clearly shows that the fingertip blood flow is densely distributed and the background is static.

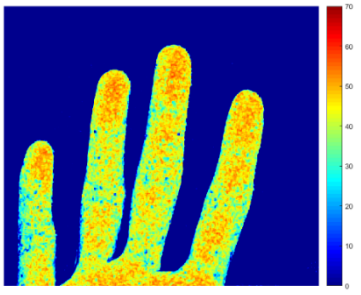

FIGURE 6. Finger microcirculation blood flow image taken by the industrial camera.

Fig. 7 shows the experimental results obtained by using a mobile phone camera. Image A clearly shows that when the effective pixels are greatly reduced, p-LSCI can show

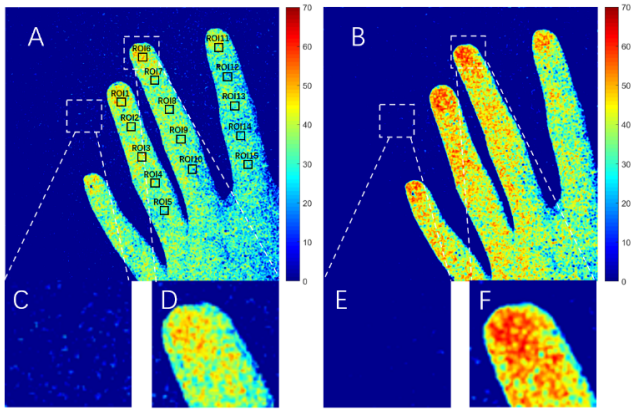

FIGURE 7. Finger microcirculation blood flow images taken by a mobile phone camera. A is the result of p-LSCI processing; B is the result of ep-LSCI processing; C and D are the enlarged p-LSCI background and fingertip images, respectively; and E and F are the enlarged ep-LSCI background and fingertip images, respectively.

only the blood perfusion in the fingertips, while the blood perfusion in other areas is not obvious. This is also due to the problem of insufficient actual lighting area and the light input of the mobile phone sensor. On this basis, reducing the effective pixels involved in the calculation will cause deviations in the calculation of the speckle contrast. Especially in some areas with weak blood flow information and edges, when the size of the original sliding window remains the same, the blurring of the speckle in this area may be weakened, thus resulting in a reduction in the gap between the area and the background and losing some blood flow information. The enlarged images E and F show that after image enhancement, the background noise is significantly reduced, the fingertip microcirculation part is clearer, and the contrast with the background is increased. To further explore the effects of the three methods on finger microcirculation detection, the CNR value and the normal distribution curve were further compared.

Fifteen ROIs were selected in Fig. 7A, and the CNR of each region was calculated using the three methods. The results were recorded in Table 3. The data in the table show that although the CNR of i-LSCI was higher than that of p-LSCI, the gap was not large. This is because during the microcirculation detection, due to the absorption and scattering of light by the skin tissue, noise will appear in the background and thus reduce the CNR of the industrial camera group. This is quite different from the simulation experiment. In contrast, the results of the ep-LSCI group were considerably improved mainly due to reducing the background noise and enhancing the microcirculation area. In addition, in the microcirculation blood perfusion experiment, the CNR fluctuated greatly, and the SD was relatively high due to the complexity of finger blood vessels. In the simulation experiment, there are fewer influencing factors, and the flow rate is fixed; therefore, the CNR obtained is relatively uniform.

Fig. 8 shows the normal distribution curve of the fingertip microcirculation area. Since there was no background noise, the contrast distribution of the i-LSCI group was more

TABLE 3. Comparison of the CNRs of the three finger microcirculation detection methods.

ROIs	i-LSCI	p-LSCI	ep-LSCI
ROI1	4.47	3.86	5.40
ROI2	4.18	3.72	4.74
ROI3	4.32	3.70	5.11
ROI4	4.14	3.55	4.50
ROI5	3.91	3.32	4.23
ROI6	4.83	4.08	5.41
ROI7	3.89	3.78	4.59
ROI8	4.07	3.93	4.72
ROI9	3.97	3.63	4.38
ROI10	3.56	3.38	4.30
ROI11	4.36	3.85	5.14
ROI12	4.00	3.27	4.02
ROI13	4.10	3.17	4.39
ROI14	3.75	3.13	4.05
ROI15	3.88	3.12	3.98
Mean	4.09	3.56	4.59
SD	0.30	0.30	0.46

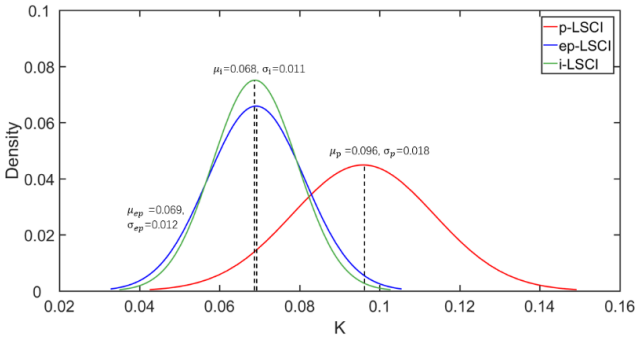

FIGURE 8. The normal distribution curve of the microcirculation area.

concentrated than that of the p-LSCI group. Compared with the p-LSCI group, the contrast distribution of the ep-LSCI group was significantly improved, and the mean was close to that of i-LSCI, thus indicating that the image from the mobile phone camera was enhanced, and the final contrast result could be closer to that of the industrial camera.

In addition, to compare whether the results of the i-LSCI and ep-LSCI detection methods are consistent, a commonly used clinical measurement evaluation method - Bland-Altman analysis [38] - was adopted. Using these two methods, we selected 100 points at the same position of the fingertips to calculate the contrast and performed a Bland-Altman analysis. In the Bland-Altman graph, the y-axis represents the difference between i-LSCI and ep-LSCI, and the red dashed line is the mean of the difference. The two methods tested are more consistent, and the dashed line representing the mean of the difference is closer to 0. The upper and lower horizontal dashed lines represent the upper and lower limits of the 95% limit of agreement (95% LoA). If the limit is clinically acceptable and the difference between the two methods is within the limit, the two methods can be considered to have good consistency [39]. The results are shown in Fig. 9. The figure shows that most of the points are within the 95% LoA, only 5% are outside the limit, and

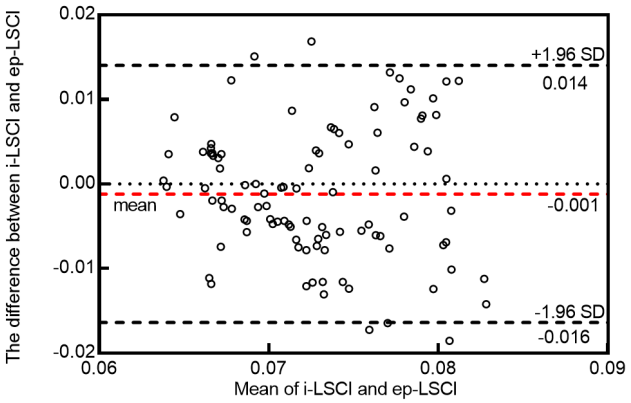

FIGURE 9. Bland-Altman graph of the contrast values of i-LSCI and ep-LSCI.

the mean line is relatively close to 0. Moreover, the maximum absolute value of the contrast difference between the two methods is 0.014, while the mean value of the contrast between the two methods is 0.072, thus having almost no influence in practical applications. Therefore, the results of i-LSCI and ep-LSCI have good consistency, and the two methods can replace each other.

IV. SUMMARY

A mobile phone camera was used to collect speckle images, and the raw speckle images were enhanced. The new method avoided the distortion caused by the mobile phone image correction algorithm and improved the speckle signal weakening due to CFA filtering. For blood perfusion detection, the ep-LSCI method not only overcomes image contrast resolution degradation but also detects some areas with weak blood flow information; these areas include tissues with small blood perfusion or small blood vessels. As the experimental results show, compared with p-LSCI, the new method can improve the CNR of the image and have a better normal distribution; thus, this method is more conducive to observing the state of blood flow and produces smaller errors when analysing and evaluating the results. Therefore, through the software method, while achieving portability of LSCI, the ep-LSCI method can also compensate for the loss of image quality caused by the device and avoid increasing the cost of the imaging device. In addition, the final result shows that the processing results of mobile phone cameras and industrial cameras still slightly differ; this difference may be caused by the different spectral responses between the cameras [40].

Although the CCD sensor used in industrial cameras has better fidelity and photosensitivity and can restore the raw speckle signal to the greatest extent, there is also little noise when detecting microcirculation blood perfusion by industrial cameras due to the absorption and scattering of light by skin tissues [41]. These noises can also be reduced by image processing. In addition, mobile phone cameras still have considerable potential in mobile medicine [42]. The CFA of sensors in mobile phone cameras also has green pixels, so these cameras have the potential to detect blood oxygen saturation. Since oxyhaemoglobin and deoxyhaemoglobin have different light absorption coefficients at different wavelengths, red and green dual-wavelength light sources can be used to irradiate fingertips to obtain different physiological information. Using a mobile phone for continuous shooting, we extracted and analysed the green and red pixel values to obtain two kinds of pulse wave signals. Then, the blood oxygen saturation was calculated according to the Beer-Lambert law by using the dual wavelength method [43].

REFERENCES

[1] L. A. Holowatz, C. S. Thompson-Torgerson, and W. L. Kenney, "The human cutaneous circulation as a model of generalized microvascular function," *J. Appl. Physiol.*, vol. 105, no. 1, pp. 370–372, Jul. 2008.
[2] S. Yuan, A. Devor, D. A. Boas, and A. K. Dunn, "Determination of optimal exposure time for imaging of blood flow changes with laser speckle contrast imaging," *Appl. Opt.*, vol. 44, pp. 1823–1830, Apr. 2005.
[3] A. F. Fercher and J. D. Briers, "Flow visualization by means of single-exposure speckle photography," *Opt. Commun.*, vol. 37, no. 5, pp. 326–330, Jun. 1981.
[4] W. Heeman, K. Dijkstra, C. Hoff, S. Koopal, J.-P. Pierie, H. Bouma, and E. C. Boerma, "Application of laser speckle contrast imaging in laparoscopic surgery," *Biomed. Opt. Exp.*, vol. 10, no. 4, pp. 2010–2019, 2019.
[5] D. Jakovels, I. Saknite, and J. Spigulis, "Implementation of laser speckle contrast analysis as connection kit for mobile phone for assessment of skin blood flow," *Proc. SPIE*, vol. 9129, May 2014, Art. no. 91293I.
[6] X. Zhang, Y. Li, H. Chen, H. Li, and S. Tong, "A low-cost and smartphone-based laser speckle contrast imager for blood flow," in *Proc. Int. Conf. Biol. Inf. Biomed. Eng. (BIBE)*, Jun. 2018, pp. 1–4.
[7] L. M. Richards, S. S. Kazmi, J. L. Davis, K. E. Olin, and A. K. Dunn, "Low-cost laser speckle contrast imaging of blood flow using a Webcam," *Biomed. Opt. Exp.*, vol. 4, pp. 2269–2283, Oct. 2013.
[8] D. Jakovels, I. Saknite, G. Krievina, J. Zaharans, and J. Spigulis, "Mobile phone based laser speckle contrast imager for assessment of skin blood flow," *Proc. SPIE*, vol. 9421, Oct. 2014, Art. no. 94210J.
[9] H. Siddiqui and C. A. Bouman, "Hierarchical color correction for camera cell phone images," *IEEE Trans. Image Process.*, vol. 17, no. 11, pp. 2138–2155, Nov. 2008.
[10] O. Yang and B. Choi, "Laser speckle imaging using a consumer-grade color camera," *Opt. Lett.*, vol. 37, no. 19, pp. 3957–3959, 2012.
[11] M. Gamadia, N. Kehtarnavaz, and K. Roberts-Hoffman, "Low-light auto-focus enhancement for digital and cell-phone camera image pipelines," *IEEE Trans. Consum. Electron.*, vol. 53, no. 2, pp. 249–257, Jul. 2007.
[12] F. Tabei, R. Zaman, K. H. Foysal, R. Kumar, Y. Kim, and J. W. Chong, "A novel diversity method for smartphone camera-based heart rhythm signals in the presence of motion and noise artifacts," *PLoS ONE*, vol. 14, no. 6, Jun. 2019, Art. no. e0218248.
[13] E. Yeom, K.-H. Nam, D.-G. Paeng, and S. J. Lee, "Improvement of ultrasound speckle image velocimetry using image enhancement techniques," *Ultrasonics*, vol. 54, no. 1, pp. 205–216, Jan. 2014.
[14] F. Lopez-Tiro, H. Peregrina-Barreto, J. Rangel-Magdaleno, and J. C. Ramirez-San-Juan, "Visualization of *in-vitro* blood vessels in contrast images based on discrete wavelet transform decomposition," in *Proc. IEEE Int. Instrum. Meas. Technol. Conf. (I2MTC)*, May 2019, pp. 1–6.
[15] H. Demirel and G. Anbarjafari, "Discrete wavelet transform-based satellite image resolution enhancement," *IEEE Trans. Geosci. Remote Sens.*, vol. 49, no. 6, pp. 1997–2004, Jun. 2011.
[16] A. Rege, K. Murari, A. Seifert, A. P. Pathak, and N. V. Thakor, "Multiexposure laser speckle contrast imaging of the angiogenic microenvironment," *J. Biomed. Opt.*, vol. 16, no. 5, 2011, Art. no. 056006.
[17] D. A. Boas and A. K. Dunn, "Laser speckle contrast imaging in biomedical optics," *J. Biomed. Opt.*, vol. 15, no. 1, 2010, Art. no. 011109.
[18] J. D. Briers, "Laser speckle contrast imaging for measuring blood flow," *Opt. Appl.*, vol. 37, pp. 1–14, Mar. 2007.
[19] C. Regan, C. K. Hayakawa, and B. Choi, "Momentum transfer Monte Carlo model for the simulation of laser speckle contrast imaging (Conference Presentation)," *Proc. SPIE*, vol. 9707, Apr. 2016, Art. no. 970703.

[20] J. D. Briers and S. Webster, "Laser speckle contrast analysis (LASCA): A nonscanning, full-field technique for monitoring capillary blood flow," *Proc. SPIE*, vol. 1, no. 2, pp. 174–180, 1996.
[21] C. E. Perez-Corona, H. Peregrina-Barreto, and J. C. Ramirez-San-Juan, "Space-directional approach to improve blood vessel visualization and temporal resolution in laser speckle contrast imaging," *J. Biomed. Opt.*, vol. 25, no. 3, Dec. 2019, Art. no. 032009.
[22] P. Miao, A. Rege, N. Li, N. V. Thakor, and S. Tong, "High resolution cerebral blood flow imaging by registered laser speckle contrast analysis," *IEEE Trans. Biomed. Eng.*, vol. 57, no. 5, pp. 1152–1157, May 2010.
[23] D. Han, "Comparison of commonly used image interpolation methods," in *Proc. 2nd Int. Conf. Comput. Sci. Electron. Eng. (ICCSEE)*, Mar. 2013, pp. 1556–1559.
[24] H. Demirel and G. Anbarjafari, "IMAGE resolution enhancement by using discrete and stationary wavelet decomposition," *IEEE Trans. Image Process.*, vol. 20, no. 5, pp. 1458–1460, May 2011.
[25] E.-S.-A. El-Dahshan, T. Hosny, and A.-B.-M. Salem, "Hybrid intelligent techniques for MRI brain images classification," *Digit. Signal Process.*, vol. 20, no. 2, pp. 433–441, Mar. 2010.
[26] S. Kumar and Y. K. Jain, "Performance evaluation and analysis of image restoration technique using DWT," *Int. J. Comput. Appl.*, vol. 72, no. 18, pp. 1–10, 2013.
[27] D. R. Nayak, R. Dash, and B. Majhi, "Brain MR image classification using two-dimensional discrete wavelet transform and AdaBoost with random forests," *Neurocomputing*, vol. 177, pp. 188–197, Feb. 2016.
[28] M. A. S. Ahmed, H. Taha, and M. T. S. Aldeen, "Image compression using Haar and modified Haar wavelet transform," *Int. J. Eng. Sci.*, vol. 18, no. 2, pp. 88–101, 2011.
[29] P. Raviraj and M. Y. Sanavullah, "The modified 2D-Haar wavelet transformation in image compression," *Middle East J. Sci. Res.*, vol. 2, no. 2, pp. 73–78, 2007.
[30] S. Zin and A. S. Khaing, "Brain tumor detection and segmentation using watershed segmentation and morphological operation," *Int. J. Res. Eng. Technol.*, vol. 3, no. 3, pp. 367–374, Mar. 2014.
[31] N. Desai, A. Singh, and D. J. Valentino, "Practical evaluation of image quality in computed radiographic (CR) imaging systems," *Proc. SPIE*, vol. 7622, Mar. 2010, Art. no. 76224Q.
[32] A. K. Dunn, "Laser speckle contrast imaging of cerebral blood flow," *Ann. Biomed. Eng.*, vol. 40, no. 2, pp. 367–377, Feb. 2012.
[33] *TXG14NIR*. Baumer, Frauenfeld, Switzerland. [Online]. Available: https://www.baumer.com/medias/__secure__/Baumer_TXG14NIR_DS_EN.pdf?mediaPK=8800949403678
[34] I. Remer and A. Bilenca, "Laser speckle spatiotemporal variance analysis for noninvasive widefield measurements of blood pulsation and pulse rate on a camera-phone," *J. Biophotonics*, vol. 8, nos. 11–12, pp. 902–907, Nov. 2015.
[35] Sony. *Image Sensor*. [Online]. Available: https://www.sony-semicon.co.jp/e/products/IS/mobile/
[36] B. K. Gunturk, J. Glotzbach, Y. Altunbasak, R. W. Schafer, and R. M. Mersereau, "Demosaicking: Color filter array interpolation," *IEEE Signal Process. Mag.*, vol. 22, no. 1, pp. 44–54, Jan. 2005.
[37] M. Rossi and A. Carpi, "Skin microcirculation in peripheral arterial obliterative disease," *Biomed. Pharmacother.*, vol. 58, no. 8, pp. 427–431, 2004.
[38] D. Giavarina, "Understanding bland Altman analysis," *Biochem. Med.*, vol. 25, pp. 141–151, Sep. 2015.
[39] C. Millet, M. Roustit, S. Blaise, and J. Cracowski, "Comparison between laser speckle contrast imaging and laser Doppler imaging to assess skin blood flow in humans," *Microvasc. Res.*, vol. 82, no. 2, pp. 147–151, 2011.
[40] F. H. Imai and R. S. Berns, "Spectral estimation using trichromatic digital cameras," in *Proc. Int. Symp. Multispectral Imag. Color Reproduction Digit. Arch.*, 1999, pp. 42–48.
[41] M. J. C. van Gemert, S. L. Jacques, H. J. C. M. Sterenborg, and W. M. Star, "Skin optics," *IEEE Trans. Biomed. Eng.*, vol. 36, no. 12, pp. 1146–1154, Dec. 1989.
[42] D. N. Breslauer, R. N. Maamari, N. A. Switz, W. A. Lam, and D. A. Fletcher, "Mobile phone based clinical microscopy for global health applications," *PLoS ONE*, vol. 4, no. 7, pp. 1–7, 2009.
[43] P. A. Kyriacou, S. Powell, R. M. Langford, and D. P. Jones, "Investigation of oesophageal photoplethysmographic signals and blood oxygen saturation measurements in cardiothoracic surgery patients," *Physiol Meas*, vol. 23, no. 3, pp. 533–545, 2002.

PING KONG received the B.S. degree in mathematics and applied mathematics from Qufu Normal University, Shandong, China, in 2001, the M.S. degree in system theory from the Kunming University of Science and Technology, Yunnan, China, in 2004, and the Ph.D. degree in management science and engineering from the University of Shanghai for Science and Technology, Shanghai, China, in 2011. Since 2011, she has been a Faculty Member with the Shanghai Key Laboratory of Molecular Imaging, Shanghai University of Medicine and Health Sciences, where she is currently an Associate Professor. Her research interest includes intelligent information processing.

HAO XU received the B.S. degree from South-Central University for Nationalities, in 2019. He is currently pursuing the M.S. degree with the School of Medical Instrument and Food Engineering, University of Shanghai for Science and Technology. His research interest includes biomedical optical imaging.

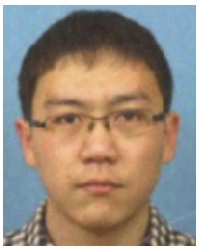

RAN LI received the bachelor's degree in communication engineering from Henan Normal University, in 2012, and the Ph.D. degree in optical engineering from the University of Shanghai for Science and Technology, in 2019. Since July 2019, he has been serving as a Postdoctoral Fellow in biomedical engineering with the University of Shanghai for Science and Technology. His research interests include high-precision optical measurement and granular matter.

GANG HUANG was born in 1961. He has served as the Director of the academic committee for the Molecular Medical Imaging Centre, MED-X Research Institute, the Appointed Chairman of the Chinese Nuclear Medicine Association, the Vice Chairman of the Shanghai Nuclear Society, and the Chairman of the Shanghai Nuclear Medicine Branch. His research interests include molecular probes and tumour imaging and omics.

WEI LIU received the Ph.D. degree in control and system theory from the Shanghai Jiao Tong University of China. From 2012 to 2014, he was a Research Assistant with the Department of Molecular, Cell and Developmental Biology, University of California, Los Angeles (UCLA), USA. He is currently an Assistant Professor with the School of Internet of Things Engineering, Binjiang College of Nanjing University of Information Science and Technology, Wuxi, China. His research interests include networks science, complex systems, computational biology, networks medicine, bioinformatics, and systems medicine.